Supporting Information for "Grain boundary diffusion of ferropericlase: Implications for the core-mantle interaction"

Yihang Peng[1], Pierre Hirel[2], Philippe Carrez[2], Jie Deng[1]

[1]Department of Geosciences, Princeton University, Princeton, NJ 08544, USA.

[2]Univ. Lille, F-59000 Lille, France.

Contents of this file

April 8, 2024, 7:50pm

Text S1.

We take pure MgO as an example to explore how the grain boundary (GB) diffusion coefficients vary with vacancy concentration (C_{vac}), system size, and the misorientation angle of the GB.

At ambient pressure with $C_{\text{vac}} \geq 3.2$ at%, the GB diffusivities in MgO for different C_{vac} show similar values within the error bars (Figure S2). Moreover, the misorientation angle likely only marginally affects the GB diffusivity (Figure S2), and the diffusivities are not sensitive to the size of the simulation system (Figure S3). We note that the present results are based on only two high-symmetry tilt GBs and other types of GB, like twist GB remain to be investigated. The diffusivity as a function of C_{vac} at high pressure is presented in Figure S5. Similar to the diffusion of Mg and O in MgO single crystals (e.g., Ammann et al., 2010), the diffusion coefficient shows a near-linear positive correlation with C_{vac} when C_{vac} is relatively low ($C_{\text{vac}} \leq 1.6$ at%). However, for $C_{\text{vac}} \geq 3.2$ at%, its facilitation effect on diffusion tends to saturate, resulting in the nearly constant GB diffusivity. Additionally, we observed that in all the systems studied, atomic diffusion occurs only within a GB region approximately 1 nm wide. Over the simulation timescale of 10–20 ns, these vacancies do not migrate into the crystal interior, thereby demonstrating strong anisotropy aligning with the findings of Riet, Van Orman, and Lacks (2018). Specifically, diffusion parallel to the GB direction (x-z plane) is the most significant (Figure S5b). Figure S6 shows the MD trajectories of Mg in the MgO GB at 4000 K and 140 GPa. It can be observed that within the 1-nm-wide GB region, some atoms no longer occupy specific crystallographic sites but show liquid-like motion. The GB transitions into a liquid-like, thermodynamically stable nanoscale film, even though the simulation temperature is below the

30 melting point. This order-disorder transition is termed GB premelting (Torabi Rad et al., 2020)

31 and has been observed in many materials (e.g., Glicksman & Vold, 1972; Dillon & Harmer,

32 2007; Frolov et al., 2013). Similar to the findings of Riet, Van Orman, and Lacks (2021) and

33 Mantisi, Sator, and Guillot (2017), the GB in this quasi-liquid state exhibits considerable disor-

34 der nature and transport properties close to those of a supercooled liquid. To further investigate

35 the evolution of the atomic structure of GBs with C_{vac}, we compare snapshots of MgO GBs

36 at various C_{vac} values during MD simulations (Figure S7). We capture the transition of the GB

37 structure from ordered to disordered as C_{vac} increased. The disorder upon reaching the limit may

38 correspond to the saturation effect observed in the GB diffusivity. This indicates that vacancies

39 within the crystal can influence the structure (Hirel et al., 2022) and diffusion characteristics of

40 the GB. However, once the GB structure stabilizes, diffusion becomes almost independent of

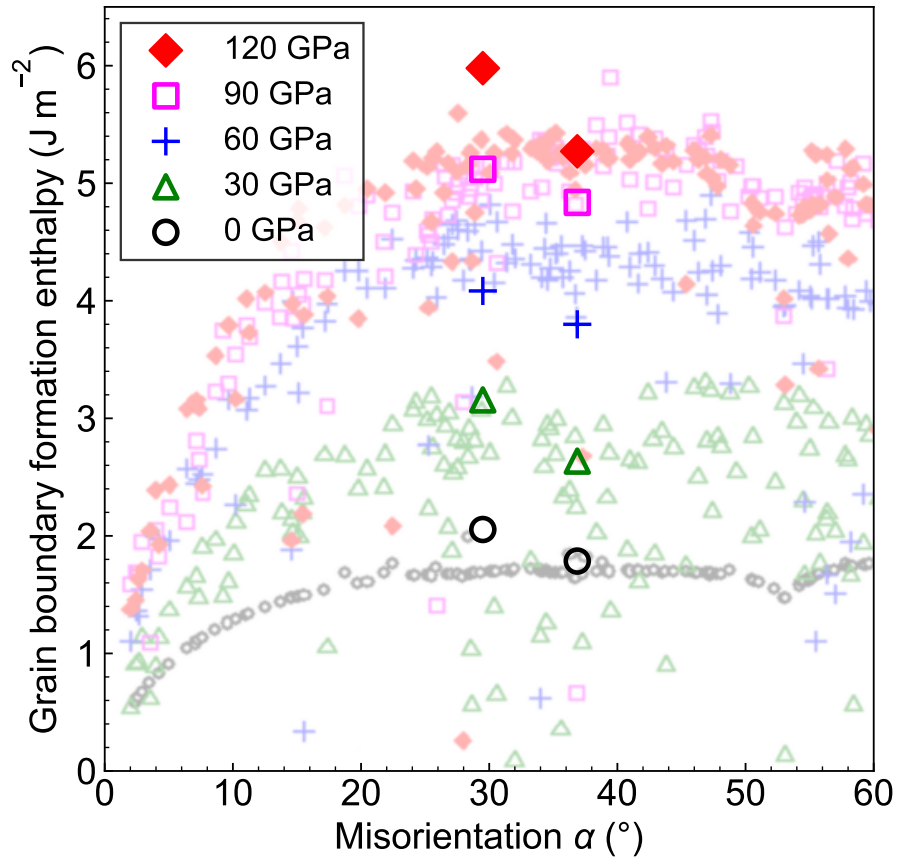41 the number of vacancies in the single crystal.

Figure S1. The formation enthalpy of [001] symmetric tilt grain boundaries in MgO as a function

of the misorientation angle at 0 GPa (black open circles), 30 GPa (green open triangles), 60 GPa (blue

crosses), 90 GPa (magenta open squares), and 120 GPa (red diamonds). The data from Hirel et al.

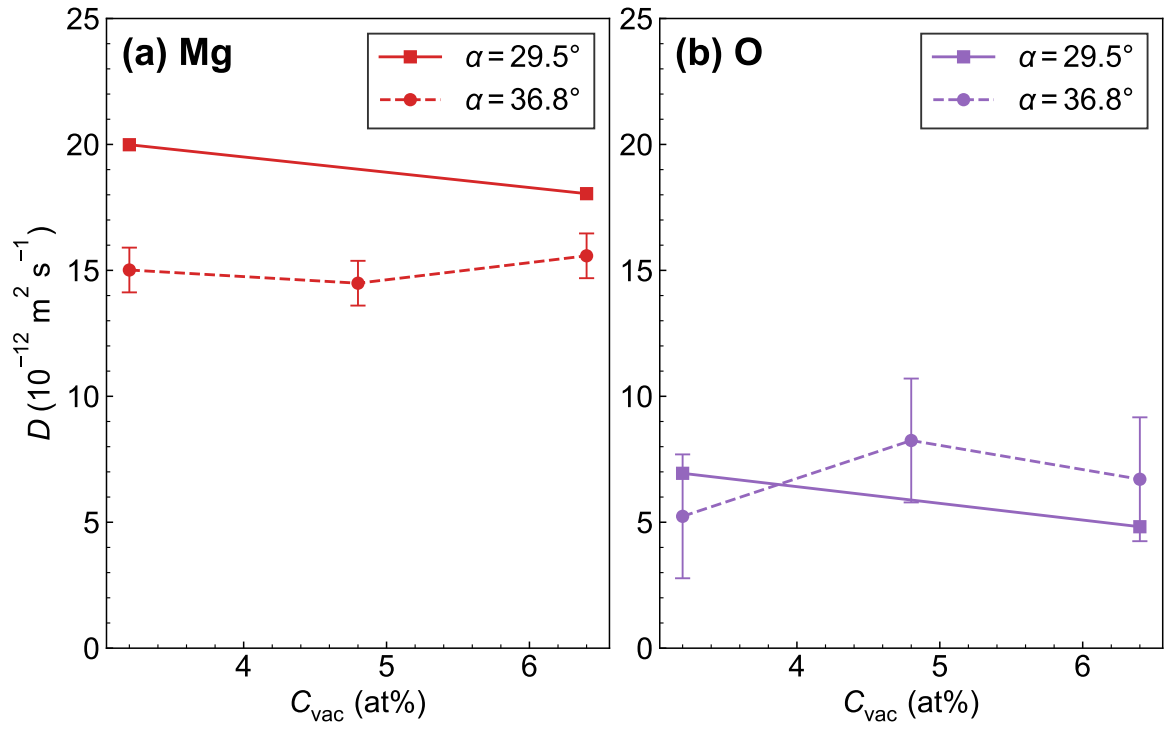(2019) are shown in light symbols for comparison.

Figure S2. Grain boundary diffusion coefficients of Mg (a) and O (b) as a function of vacancy concentration for two different misorientation angles (α) at 2000 K and 0 GPa. The error bars for $\alpha = 36.8°$ are the 2SD values for the diffusivity data with different vacancy concentrations.
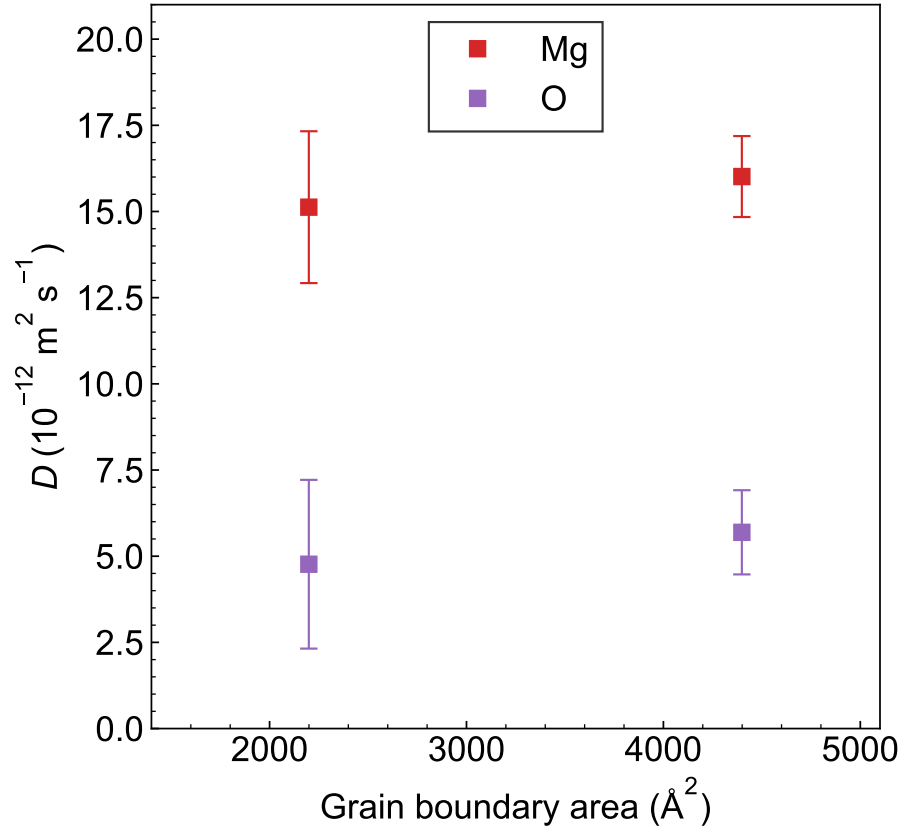
Figure S3. Grain boundary diffusion coefficients of Mg (red) and O (purple) as a function of the area of the grain boundary in the simulation box at 2000 K and 0 GPa. The larger supercell (grain boundary area: 4398.5 Å^2) is obtained by duplicating the smaller supercell (grain boundary area: 2199.3 Å^2) along the z-axis twice. The error bars are given by the differences of the results from two 5-ns trajectories.
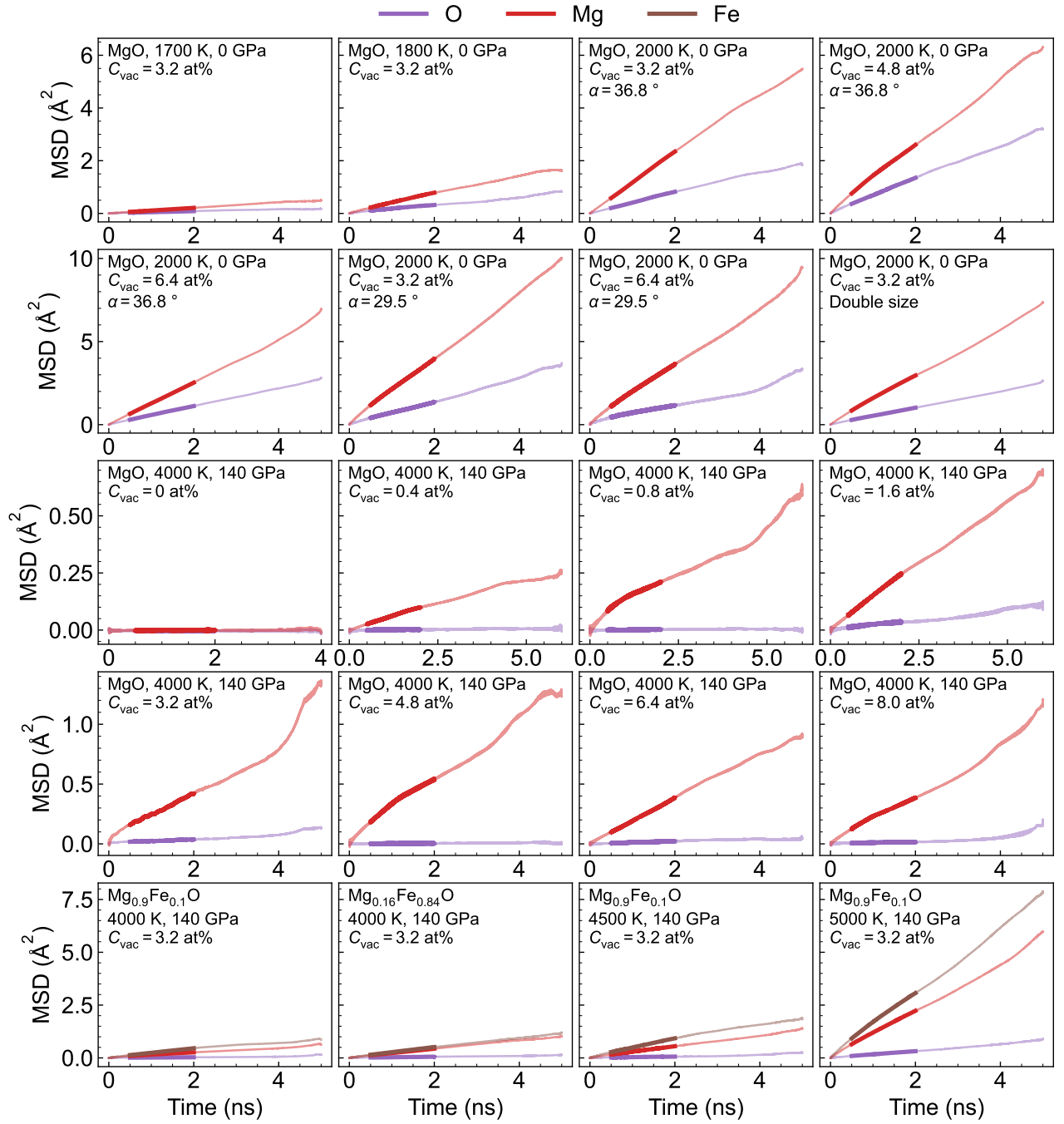
Figure S4. The mean square displacements (MSDs) as a function of simulation time for all diffusion coefficients calculated in this study. The chemical composition, temperature (T), pressure (P), and vacancy concentration (C_{vac}) are listed for all systems. The misorientation angle (α) is listed for systems in Figure S2. Average MSDs are shown for systems with multiple trajectories. Thick lines represent the sections used for linear fitting.
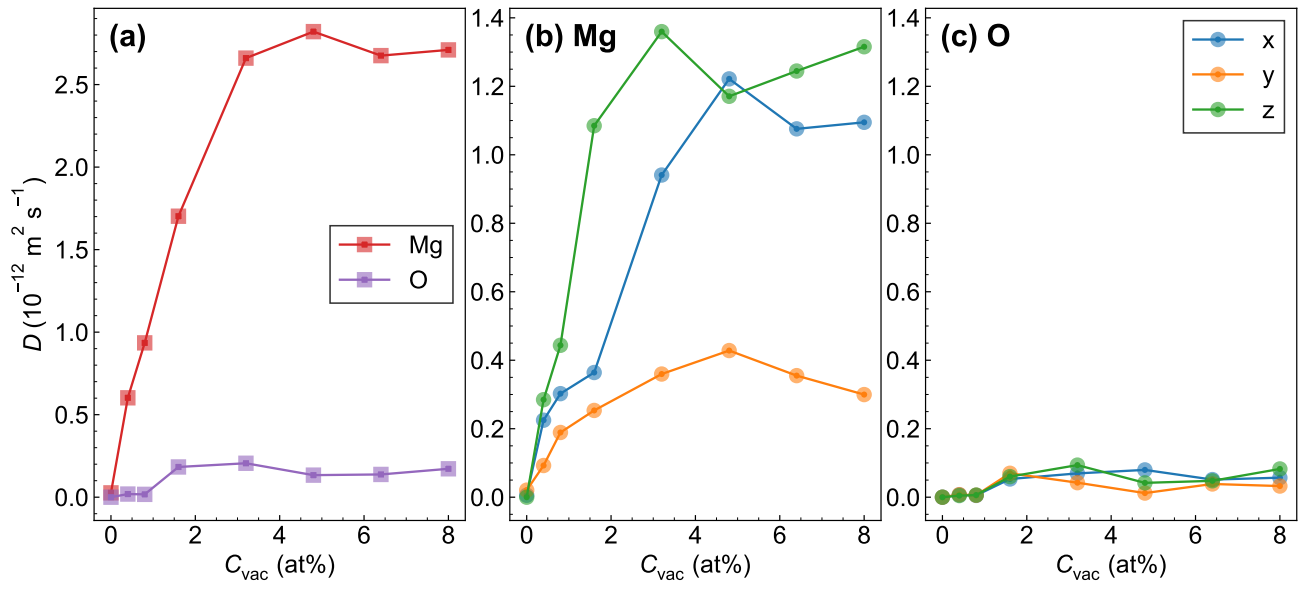
April 8, 2024, 7:50pm

Figure S5. (a) The grain boundary diffusion coefficients of Mg (red) and O (purple) as a function of vacancy concentration for MgO at 140 GPa and 4000 K. (b, c) The anisotropy of grain boundary diffusion of Mg (b) and O (c) shown by plotting diffusion coefficients along three axes, x (blue), y (orange), and z (green).
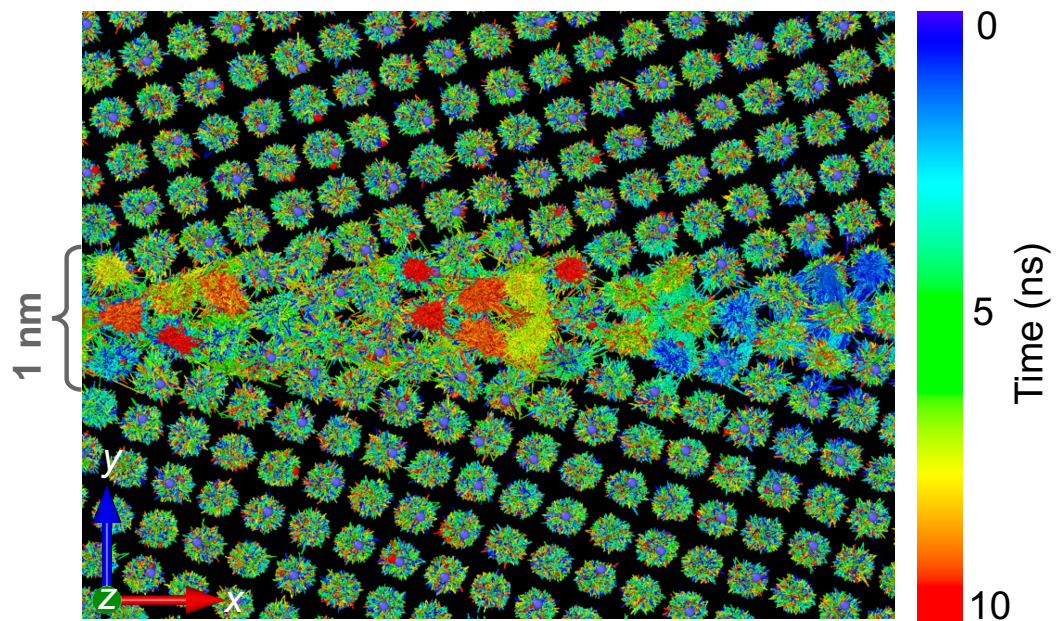
Figure S6. Color mapping of the trajectories of Mg over time in polycrystalline MgO ($C_{vac} = 3.2$ at%) at 4000 K and 140 GPa. As the simulation time increases from 0 ns to 10 ns, the color of the trajectory changes along the visible spectrum.
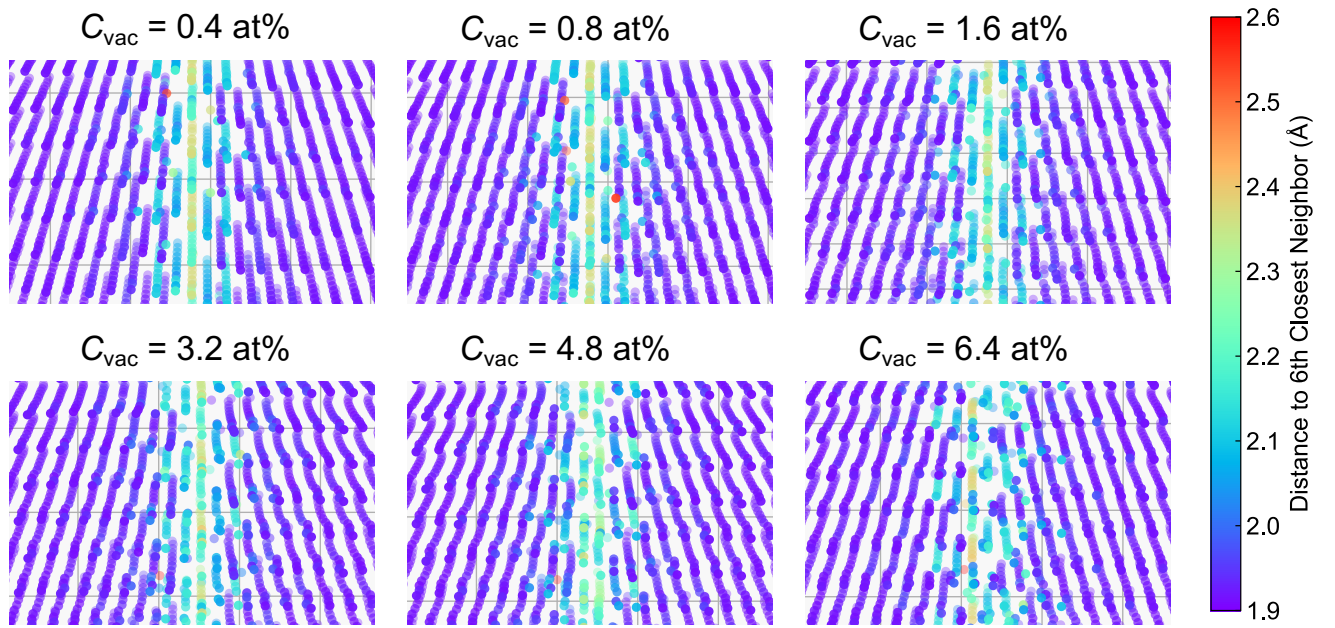
Figure S7. The evolution of grain boundary structure of MgO as a function of vacancy concentration at 4000 K and 140 GPa. The colors of atoms are obtained by mapping the distance from each atom to its 6th nearest neighbor. All snapshots are taken at 1 ns of the MD simulations and relaxed by energy minimization.

References

Ammann, M. W., Brodholt, J. P., Wookey, J., & Dobson, D. P. (2010). First-principles constraints on diffusion in lower-mantle minerals and a weak D″ layer. *Nature*, *465*(7297), 462–465. doi: 10.1038/nature09052

Dillon, S. J., & Harmer, M. P. (2007, September). Multiple grain boundary transitions in ceramics: A case study of alumina. *Acta Materialia*, *55*(15), 5247–5254. doi: 10.1016/j.actamat.2007.04.051

Frolov, T., Olmsted, D. L., Asta, M., & Mishin, Y. (2013, May). Structural phase transformations in metallic grain boundaries. *Nature Communications*, *4*(1), 1899. doi: 10.1038/ncomms2919

Glicksman, M. E., & Vold, C. L. (1972, June). Heterophase dislocations — An approach towards interpreting high temperature grain boundary behavior. *Surface Science*, *31*, 50–67. doi: 10.1016/0039-6028(72)90253-1

Hirel, P., Carrez, P., & Cordier, P. (2022, November). Why do compact grain boundary complexions prevail in rock-salt materials? *Acta Materialia*, *240*, 118297. doi: 10.1016/j.actamat.2022.118297

Mantisi, B., Sator, N., & Guillot, B. (2017, December). Structure and transport at grain boundaries in polycrystalline olivine: An atomic-scale perspective. *Geochimica et Cosmochimica Acta*, *219*, 160–176. doi: 10.1016/j.gca.2017.09.026

Riet, A. A., Van Orman, J. A., & Lacks, D. J. (2018, November). The interplay of structure and dynamics at grain boundaries. *The Journal of Chemical Physics*, *149*(19), 194501. doi: 10.1063/1.5052188

Riet, A. A., Van Orman, J. A., & Lacks, D. J. (2021, January). A molecular dynamics study of grain boundary diffusion in MgO. *Geochimica et Cosmochimica Acta*, *292*, 203–216. doi: 10.1016/

63   j.gca.2020.09.012

64   Torabi Rad, M., Boussinot, G., & Apel, M. (2020, December). Dynamics of grain boundary premelt-

65   ing. *Scientific Reports*, *10*(1), 21074. doi: 10.1038/s41598-020-77863-9